Theory of electronic structure and magnetic behavior of fcc iron grown on Cu(001)

Gayanath W. Fernando
Department of Physics, Brookhaven National Laboratory, Upton, New York 11973-5000

Bernard R. Cooper
Department of Physics, West Virginia University, Morgantown, West Virginia 26506
and Center for Materials Science, Los Alamos National Laboratory, Los Alamos, New Mexico 87545
(Received 29 February 1988)

The self-consistent film linearized muffin-tin-orbital method has been used to calculate the magnetically ordered and paramagnetic electronic structure of fcc iron as grown on Cu(001). Some recent experimental and theoretical work on this system is critically examined. Our calculations indicate that the zero-temperature ground state of this system has an antiferromagnetic interior and ferromagnetic coupling at the surface with an enhanced surface magnetic moment of $2.8\mu_B$.

I. INTRODUCTION

Understanding the stability of various crystal phases and their electronic and magnetic properties from first principles is a problem of central importance in solid-state physics. This is especially challenging in iron because of its rich variety of phases, both magnetically ordered and paramagnetic. Although its low-temperature and low-pressure ferromagnetic phase (α-iron) has been studied extensively, not much is known about its other phases, such as the close-packed (fcc) γ phase. Under normal conditions iron is bcc (α phase). At $T_C = 1041$ K it transforms to another bcc (β) phase, which is paramagnetic. Transformation to the fcc γ phase occurs at a slightly higher ($T = 1183$ K) temperature. Iron goes through a third bcc δ phase before melting at 1811 K. All of the above transition temperatures are for atmospheric pressure. Iron also has a high-pressure hcp ϵ phase. Various attempts have been made to understand the phase diagram of iron. For example, Hasegawa and Pettifor[1] have shown through a microscopic theory that the magnetic contributions to the free energy are responsible for these various phase transitions.

The magnetic nature of fcc γ-iron deposited on copper substrates has been of great interest for quite some time. Early experiments on this system showed ferromagnetic sheets coupled antiferromagnetically to each other with size-dependent Néel temperatures.[2] More recent work claimed to show ferromagnetism (Refs. 3–5) or its absence at room temperature (Refs. 6–10) through various methods such as Mössbauer spectroscopy and photoemission spectroscopy. The low-temperature magnetic state of these films has been reported as antiferromagnetic.[10] The ability to prepare quality single-crystal films of fcc iron on copper substrates has been demonstrated recently by various experimental groups (Refs. 3–8), although there is no general agreement with regard to the magnetic state at room temperature. Utilizing improved techniques of epitaxial growth and techniques such as [6,7] high-resolution low-energy electron diffraction (LEED) and Auger spectroscopy under ultra high-vacuum conditions, the experimentalists have been able to stabilize and monitor the growth process of iron on Cu(001) which is generally believed to be a layer-by-layer growth. On the theoretical front, fcc iron has attracted much attention in part because of predictions of transitions between different magnetic states with increasing lattice parameter (Refs. 11–16). Most of this work qualitatively agrees about the nature of the transition, but the transition lattice-parameter values vary between different workers. Whether magnetic or nonmagnetic, ability to grow these epitaxial films has provided a unique opportunity to study a phase of iron, otherwise unstable at room and lower temperatures.

II. METHOD

The calculational method employed here is the recently perfected self-consistent film linearized muffin-tin-orbital (FLMTO) method,[17] which has been tested on a variety of $3d$ and $4d$ transition-metal slabs to yield accurate work functions and spectroscopic features. The main advantage of this method over other accurate band-structure methods, such as the linearized augmented-plane-wave (LAPW) method, is its inherently small basis set. As one proceeds to study systems with a large number of atoms in the unit cell, methods that use large bases such as the LAPW method become impractical. The basis functions used here are a combination of the standard muffin-tin orbitals (MTO's) and additional independent functions called plane-wave orbitals (PWO's). The MTO's are labeled by indices α for the given atom and (l,m) for the angular momentum. The MTO's inside the spheres consist of a linear combination of the solution of the radial Schrödinger equation and its energy derivative for the spherically averaged actual potential. In the interstitial region the MTO is a Hankel function, while in the vacuum it consists of a linear combination of the one-dimensional (1D) Schrödinger solution and its energy derivative for the vacuum potential averaged over the plane-parallel direction. The PWO's are defined as 2D (two-dimensional) plane waves in the parallel (to the sur-

face) direction. Along the inward normal to the surface they either have a real exponential behavior or a plane-wave-like behavior, depending on the value of an energy parameter κ and the parallel reciprocal-lattice vector. These are augmented, as are the MTO's inside the sphere and the vacuum regions (using linear combinations of the appropriate one-dimensional Schrödinger solution and its energy derivative for the corresponding averaged potential) and used as independent functions to expand the wave function together with the MTO's. These functions are continuous and have continuous first derivatives everywhere. The variational freedom in this expanded set is certainly higher than that of a pure MTO basis, but still the basis-set size can be kept fairly small while yielding quality results. (As discussed in Sec. III, for paramagnetic five-layer fcc Cu or Fe, 45 MTO's plus 18 PWO's are sufficient, while for seven-layer paramagnetic Fe on Cu, 63 MTO's are sufficient and the number of PWO's necessary remains at 18).

We use the full potential everywhere except inside the spheres. The non-muffin-tin (NMT) potential in the spheres is approximated by the extended interstitial NMT potential as described in Ref. 17. This is exact at the sphere boundary, and hence clearly a good approximation in the region just inside the sphere boundary where the non-muffin-tin effects are significant. We note that the full potential [higher (l,m) components of the potential] inside the spheres can readily be accommodated here, as the basis functions are defined according to (l,m) values and hence the method is ideally suited for such an extension. The valence electrons are treated semirelativistically ignoring the spin-orbit interaction, while the core is calculated from the full Dirac equation and is allowed to relax while iterating so that we may calculate core-level shifts. The Fourier-series cutoff $G_{\max}$ is about $6.5a_0^{-1}$ (a_0 being a Bohr radius). The correlation potential used in the magnetic and nonmagnetic cases is the parametrization of Vosko, Wilk, and Nusair.[18] The iterative self-consistent procedure is carried on until the input and the output potential difference is of the order of a few mRy or less everywhere in space.

For the spin-polarized case it is useful to define a variable η corresponding to the spin-up ($\rho^{\uparrow}$) and spin-down ($\rho^{\downarrow}$) charge densities as

$$\eta=\frac{\rho^{\uparrow}-\rho^{\downarrow}}{\rho^{\uparrow}+\rho^{\downarrow}} . \tag{2.1}$$

To start the spin-polarized calculation from the non-spin-polarized case we choose an η giving rise to a splitting of a few mRy in the potential. Then, two independent Schrödinger equations corresponding to the split potentials, $V^{\uparrow}$ and $V^{\downarrow}$, are solved at each k point to obtain the corresponding eigenvalues and eigenvectors. The occupied eigenstates will, in turn, give rise to two charge densities $\rho^{\uparrow}$ and $\rho^{\downarrow}$ corresponding to the spin-up and spin-down electrons. At this stage the output densities are mixed with the input densities as explained in the next paragraph. The resulting total charge density $\rho=\rho^{\uparrow}+\rho^{\downarrow}$ is used to calculate the Coulomb potential V_C, while both ρ and η are used to calculate the exchange-correlation potentials $V_{\rm xc}^{\uparrow}$ and $V_{\rm xc}^{\downarrow}$. [η is specified in the first few iterations and calculated from Eq. (2.1) thereafter]. The self-consistent procedure could now be continued using the new potentials,

$$V^{\uparrow}(\rho,\eta)=V_C(\rho)+V_{\rm xc}^{\uparrow}(\rho,\eta) \tag{2.2}$$

and

$$V^{\downarrow}(\rho,\eta)=V_C(\rho)+V_{\rm xc}^{\downarrow}(\rho,\eta) . \tag{2.3}$$

It should be noted that since we ignore the spin-orbit interaction in the valence electrons, our calculations cannot specify a spatial direction for the resulting magnetic moments.

Mixing the input and output densities (or potentials) is an essential step in the self-consistent process to obtain an input density (or a potential) for the next iteration which will move the system closer to the self-consistent solution. We have used potential mixing in the nonmagnetic case and charge mixing in the magnetic case. The potentials or total charge densities are mixed using straight (addition of a fraction δ of the output to a fraction $1-\delta$ of the input) or Broyden[19] mixing schemes with mixing parameters around 2–4 % (of the output). These mixing parameters have to be kept small since surface calculations are extremely sensitive to small changes in the charge densities. However, it is possible to use a large mixing percentage β when the spin densities, $s=\rho^{\uparrow}-\rho^{\downarrow}$, are mixed, i.e.,

$$s_{\rm input}^{j+1}=\beta s_{\rm output}^{j}+(1-\beta)s_{\rm input}^{j} , \tag{2.4}$$

where β can be as high as 80%. Here, j and $j+1$ refer to two successive iterations. This spin mixing, together with an appropriate charge mixing, can move the system rapidly towards the self-consistent solution.

III. RESULTS OF CALCULATIONS

A. Slab systems treated

Our calculations were motivated by the recent experiments on iron epitaxially grown on Cu(001). It has been possible to grow iron films up to a fairly substantial number of layers on Cu(001) and this has provided a unique opportunity for studying bulk as well as surface properties of fcc iron at room temperature. Auger spectroscopy and LEED have been used to identify the growth process and to determine the lattice structure. There is agreement among various experimental groups as to the crystal structure, which is fcc, and the lattice constant, which is that of fcc copper. As the film thickness increases to, say, more than 10 layers, there are problems with impurities, and for even thicker films the expected transition to bcc iron occurs. A major reason for being able to stabilize thick iron films on Cu(001) is the close match of the fcc lattice constants of these two $3d$ metals.

The calculations were done for thin slabs of fcc iron and iron on Cu(001) using the lattice constant of fcc Cu ($=6.83a_0$). All the slabs considered have z (normal to the slab) reflection symmetry with respect to the central plane and an odd number of layers. The film geometry

(i.e., separation into sphere, interstitial, and vacuum regions) is as discussed in Ref. 17. No surface relaxations were included for fcc iron where a five-layer film was used with five atoms in the unit cell, i.e., one atom per (001) layer. For this slab both magnetic and nonmagnetic calculations were performed. The choice of the unit cell precludes antiferromagnetism within a layer, so the only ordering possible within a layer is ferromagnetic, but between the layers the system has the freedom to choose its magnetic orientation. For the system Fe/Cu a monolayer of iron on each side of a five-layer film of fcc Cu(001) was considered with iron occupying the fourfold hollow sites as a continuation of the copper lattice. The self-consistent calculations were also performed for this same slab with a slightly expanded (2%) surface-subsurface interlayer spacing. For comparisons we also used calculations for[17] a five-layer slab of fcc Cu(001). The Fe-on-Cu and Cu calculations were done only for the paramagnetic state. All these systems have rotational symmetry C_{4v} about the surface normal through a given atom and a square Brillouin zone. Special k points were used in the irreducible $\frac{1}{8}$ of the Brillouin zone totaling up to 28 in the final iterations towards self-consistency. The basis-set sizes were 63 for the five-layer film (45 MTO's and 18 PWO's) and 81 for the seven-layer film (63 MTO's and 18 PWO's).

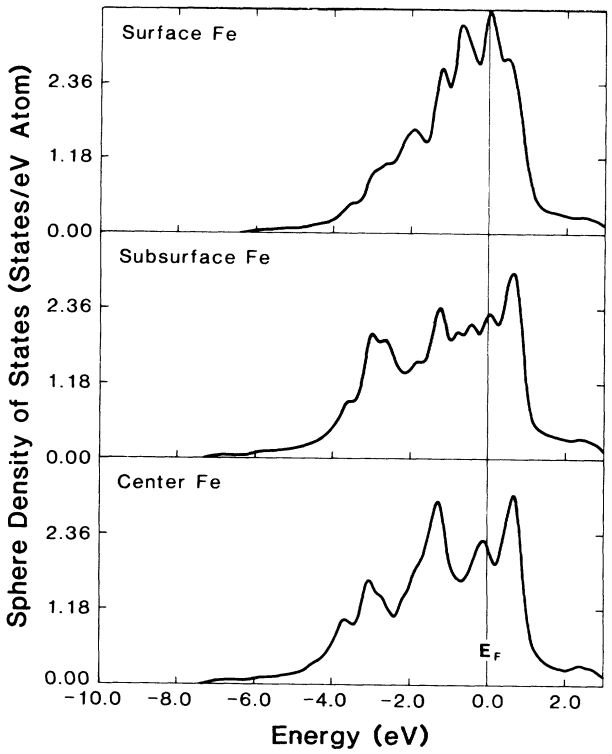

FIG. 1. Layer-projected paramagnetic density of states for fcc iron. These have been smoothed by a Gaussian of full width at half maximum (FWHM) of 0.3 eV. The lattice constant used here is that of Cu ($6.83a_0$). The high density of states at the Fermi level makes it an ideal candidate to satisfy the Stoner criterion to become magnetically ordered.

B. Density of states and band structure

Our calculated nonmagnetic density-of-states (DOS) curves for the fcc Fe(001) five-layer slab and for Fe/Cu(001) are shown in Figs. 1 and 2. Two striking features present in these DOS are (1) the narrowing of the surface iron density of states, and (2) the sharp peaks at the Fermi level in the paramagnetic iron DOS. The narrowing of the surface iron DOS is due to reduced coordination at the surface. The loss of neighbors of the surface atom makes its potential less attractive compared to the inner-layer potentials and (with a resulting net increase in energy eigenvalue with the inclusion of the kinetic part) the states are pushed to less negative energies. The sharp peaks present in the paramagnetic iron atoms are almost entirely due to d electrons. Unlike in Cu, the d states are not fully occupied in iron and this allows the Fermi level to cut through d-like states, and a high DOS at the Fermi level makes it an ideal candidate to satisfy the Stoner criterion, i.e., it could be energetically favorable to order into a magnetic state by making use of the exchange interaction. In fact, as we shall see later, for the fcc iron slab this turns out to be the case.

The DOS curves shown (by the solid curves) in Fig. 2 are for the unrelaxed Fe/Cu system. The (2%) relaxed system has a DOS almost identical to that shown here. In Fig. 2 we also show a layer-projected fcc Cu(001) five-layer DOS (dashed lines) to compare to the Fe/Cu(001) DOS. The electronic screening of the surface effects is very rapid, as can be seen here. Two layers below the surface, the Cu DOS looks very much like the bulk. Also, the surface Cu DOS gets broader and moves towards higher binding energies when a monolayer of iron is deposited on it. This is an indication of the d-d bonding that takes place between iron and copper. We also see differences between the surface iron DOS from the five-layer fcc iron slab and the surface iron DOS from the system Fe/Cu in the energy range 2–4 eV below the Fermi level. These are most likely to be due to the different d-level placements in Cu compared to Fe, which determine the eventual d-d–bonding–level placements in Fe-Cu and Fe-Fe.

The spin-polarized fcc iron five-layer DOS curves are shown in Fig. 3. As can be seen from this figure, the center-layer moment is aligned antiferromagnetically to the surface- and subsurface-layer moments. Our total-energy calculations predict this to be the magnetic ordering of the ground state, as will be discussed later. The surface-atom majority-spin d states are all occupied, while the minority states show only a partial occupation. This contrast between the majority- and the minority-spin occupation is strongest at the surface atom and hence it will give rise to an enhanced magnetic moment at the iron surface. *The occupation of more antibonding majority states at the surface at the expense of bonding minority states will energetically favor an expanded lattice near the surface region with the onset of magnetic ordering.* It is also interesting to examine the magnetic splittings and the shapes of the majority and minority DOS

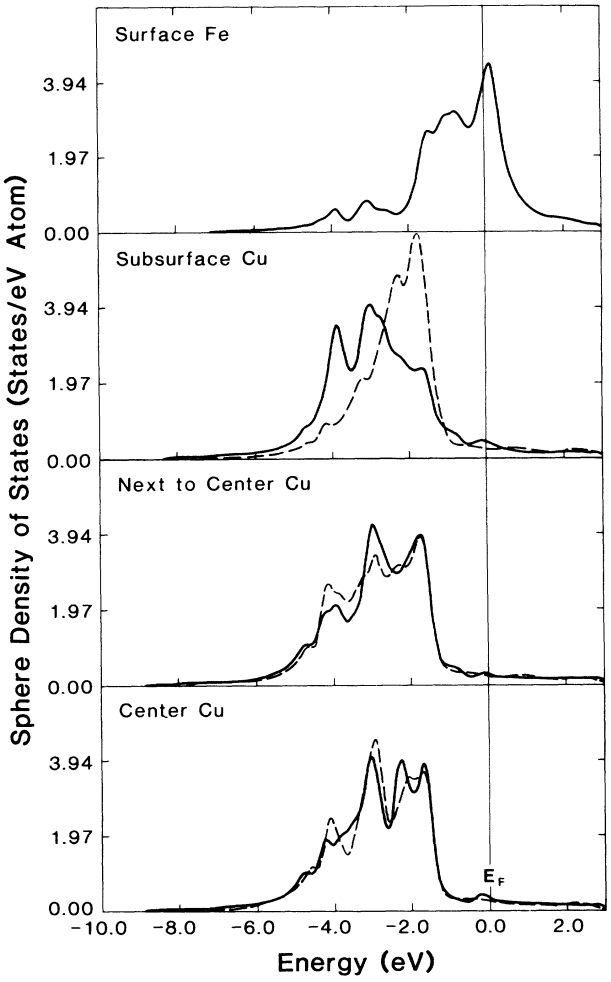

FIG. 2. Layer-projected density of states for Fe/Cu(001) and Cu(001) shown by solid and dashed lines, respectively. The lattice constant and the smoothing are the same as in Fig. 1. Note how the narrow Cu-surface-atom density of states gets broader and pushed to higher binding energies when a monolayer of iron is deposited on it.

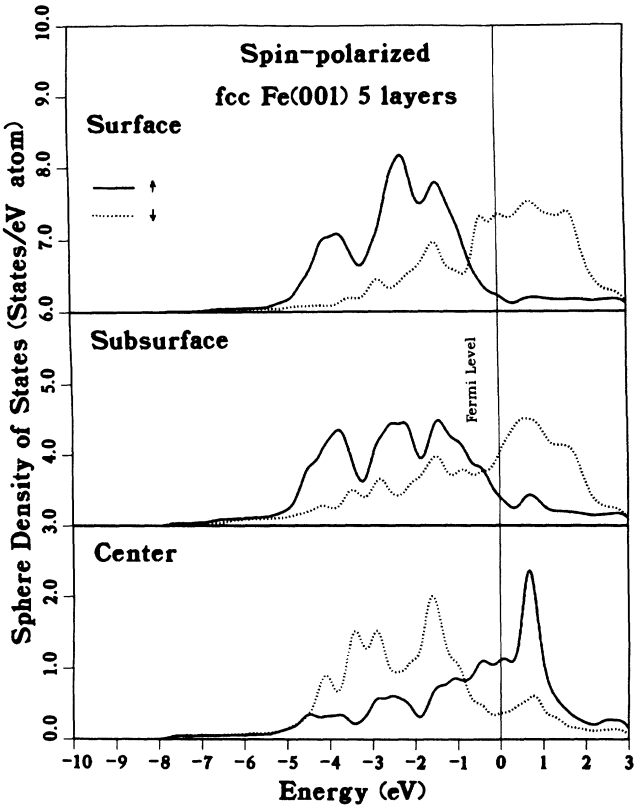

FIG. 3. Layer-projected spin-polarized density of states for fcc iron. The lattice constant and the smoothing are the same as in Fig. 1. The solid lines show a spin-up density of states, while the dotted lines show the spin-down density of states. Note that the surface spin-up (majority) *d* states are all occupied and also that the center-layer net moment is aligned antiferromagnetically to those of the surface and subsurface layers.

curves. The splitting seen is clearly not a rigid uniform shift of majority states to higher (and minority states to lower) binding energies. There are other (hybridizing-type) effects that take place between the *d* orbits that shift due to magnetic ordering, giving rise to somewhat different features in the DOS compared to the nonmagnetic case. The different shapes in the DOS curves in the magnetic and nonmagnetic cases are due to different level placements, polarizabilities, and hybridization effects associated with the states in question. One can also make a rough estimate of about 2.5 eV for the bulk exchange splitting by comparing the corresponding minority and majority peaks of the center-layer DOS.

Our calculated bands for the nonmagnetic and magnetic fcc iron five layers are shown in Figs. 4 and 5. These are separated into even and odd symmetries with respect to the mirror plane along the particular high-symmetry direction being examined. Solid and dashed lines here refer to another symmetry present in our calculations, namely the *z* reflection symmetry through the central (slab) plane. Darkened lines in these figures show bands that have more than 50% weight from the surface atoms. In the paramagnetic case there are many surface-dominated bands around the Fermi level, while in the spin-polarized case there are not that many. For the majority-spin bands in both even and odd symmetries there is a substantial downward (to higher binding energies) shift of surface-dominated bands. There is also a similar upward shift for the surface-dominated minority-spin bands giving rise to a depletion in the DOS around the Fermi level. The exchange-interaction energy gained by occupying more states having the same spin orientation is apparently more than any increase in kinetic energy for the states that were close to the Fermi level in the paramagnetic case. The shifts in these bands are around 1 eV or more when the Fermi levels of the magnetic and nonmagnetic cases are aligned, giving rise to splittings of the order of 2 eV or more. We also note that the magnetic splitting shows a strong dependence on the orbital type. For example, the lowest-lying 4*s* state at -7.7 eV at $\bar{\Gamma}_1$ [Figs. 5(a) and 5(b)] shows hardly any splitting,

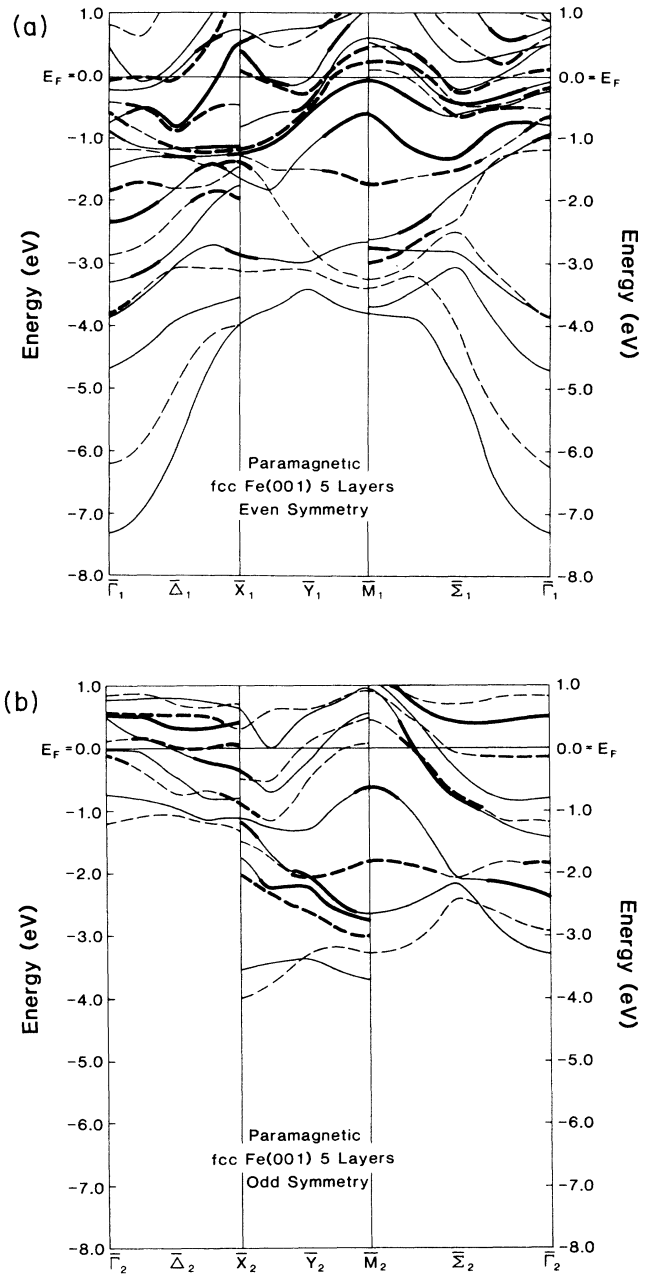

FIG. 4. Calculated paramagnetic bands for a fcc iron (001) five-layer slab. The solid and dashed lines refer to + and − z (normal to the slab) reflection symmetries, respectively. The darkened solid and dashed lines indicate states where the surface Fe weight is more than 50%. The even and odd symmetries in (a) and (b) refer to reflections about mirror planes through the corresponding high-symmetry directions.

while the lowest-lying t_{2g}-type state at −2.2 eV [Fig. 5(c)] at $\bar{\Gamma}_2$ has undergone a splitting of about 2.3 eV, i.e., the corresponding minority-spin t_{2g} state is at 0.1 eV above the Fermi level [Fig. 5(d)]. There appears to be a net gain in absolute energy of these single-particle levels due to spin polarization, provided that the difference in the work functions of the magnetic and nonmagnetic cases is small. However, the total energy consists of many other terms in addition to the single-particle energies, and a final determination of the ground state results from a careful evaluation of all those terms.

In Fig. 6 we present a *"film-derived bulk band structure"* that has been calculated using the paramagnetic fcc iron five-layer energy eigenvalues at $\bar{\Gamma}$ and their symmetries. The open circles are those calculated states and the solid line is a guide to the eye. The lowest-lying band here is the iron 4*s* band. The rest (including the dashed line) constitute five *d* bands. The degeneracy of the Δ_5 band is preserved since in the slab calculation d_{xz} and d_{yz} states are degenerate at $\bar{\Gamma}$. The splitting of about 0.4 eV seen between the Γ_5 and $\Gamma_{2'}$ states will not be present in any true bulk calculation (i.e., they will be degenerate at Γ). The splitting seen here is solely due to the presence of the surface. The band represented by the dashed line is the only band that looks significantly different from a true bulk band structure[11] and the reason here is that most of the states belonging there are highly-surface-dominant ones and hence very different from bulklike states. We will later compare these, and also our 2D bands, with available experimental results.

Some general observations for the spin-polarized bands and DOS we have calculated are the following. (1) The majority-spin, surface *d* bands are all occupied and hence a large moment should be seen for the surface atom. (2) The exchange splitting is largest for the surface-dominated bands near the Fermi level. Band narrowing due to the reduced coordination at the surface and the high-Fermi-level DOS in the surface atom naturally leads to Stoner-type itinerant magnetism here. (3) The occupation of more antibonding surface majority bands at the expense of bonding minority bands should lead to an expanded lattice in the surface region compared to bulk. This expansion will be in addition to any surface expansion (see Refs. 6 and 7) present in a paramagnetic state, and should be observable through the ordering temperature with LEED. (4) The spin-polarized surface iron atom does not show a strong narrowing of the DOS as seen in the nonmagnetic case, indicating that a strong exchange interaction can make the narrowing effect less pronounced.

C. Work functions and electron densities

Table I shows a list of experimental and theoretical work functions for the system iron grown on Cu(001) and total charges and net moments inside muffin-tin spheres in various layers. The calculated paramagnetic work function for fcc iron, 5.3 eV, as well as for Fe/Cu(001) agrees well with the experimental value at room temperature.[6,7] There is a small decrease in the work function in the paramagnetic case upon going from a monolayer of iron on Cu(001) to five layers of fcc Fe(001). The Fe/Cu(001) work function is significantly larger than the copper work function, implying that the monolayer of iron has induced an increased surface dipole barrier. Our calculated electron-density contour maps (Fig. 7) show a charge transfer toward the surface in going from Cu(001)

to Fe/Cu(001). These difference-density contours are calculated by subtracting a self-consistent Cu(001) five-layer film density from our Fe/Cu(001) electron density by aligning the surface layers of the two films. The main reason for doing this was to compare the surface electron densities of Cu(001) and Fe/Cu(001) and not to look for any bonding-type changes. It is also interesting to see the increase in the interstitial electron density, which is likely to be due to less localized orbitals in iron compared to Cu.

The magnetic fcc iron surface has a slightly reduced calculated work function compared to the nonmagnetic case and agrees favorably with the experimental value for the magnetic state seen[6,7] at 460 K. However, in judging the significance of this change it should be remembered that any increase in temperature is known usually to decrease the work function. Although the calculated work functions for fcc iron differ by about 0.2 eV between the magnetic and nonmagnetic cases, the calculated total charges inside the muffin-tin spheres stay almost con-

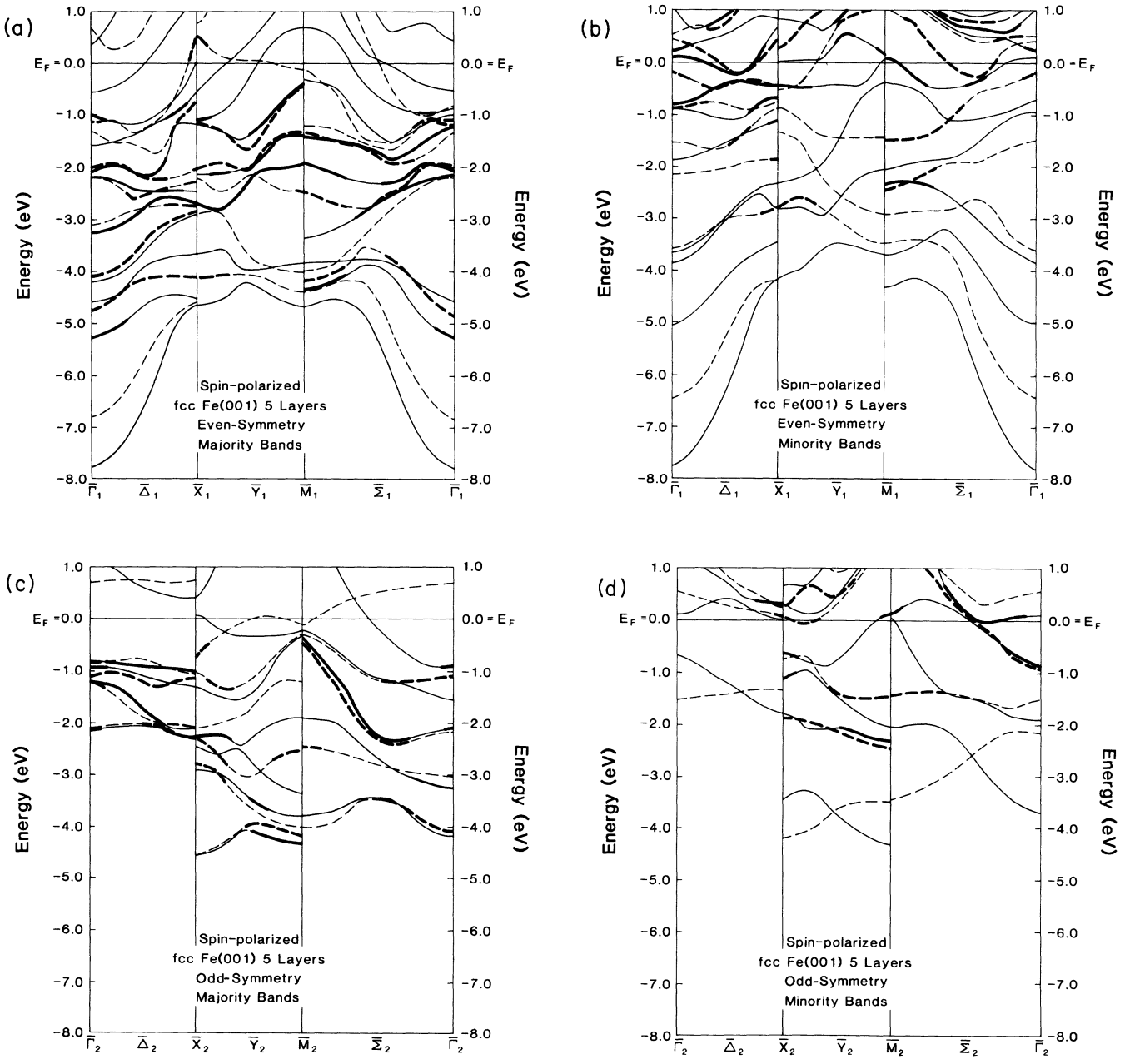

FIG. 5. Calculated spin-polarized bands for a fcc iron (001) slab. (a) Even-symmetry majority bands. (b) Even-symmetry minority bands. (c) Odd-symmetry majority bands. (d) Odd-symmetry minority bands. The solid and dashed lines refer to + and − z (normal to the slab) reflection symmetries. The darkened solid and dashed lines show states where the surface Fe weight is more than 50%. The even and odd symmetries refer to reflections about the mirror planes through high-symmetry directions.

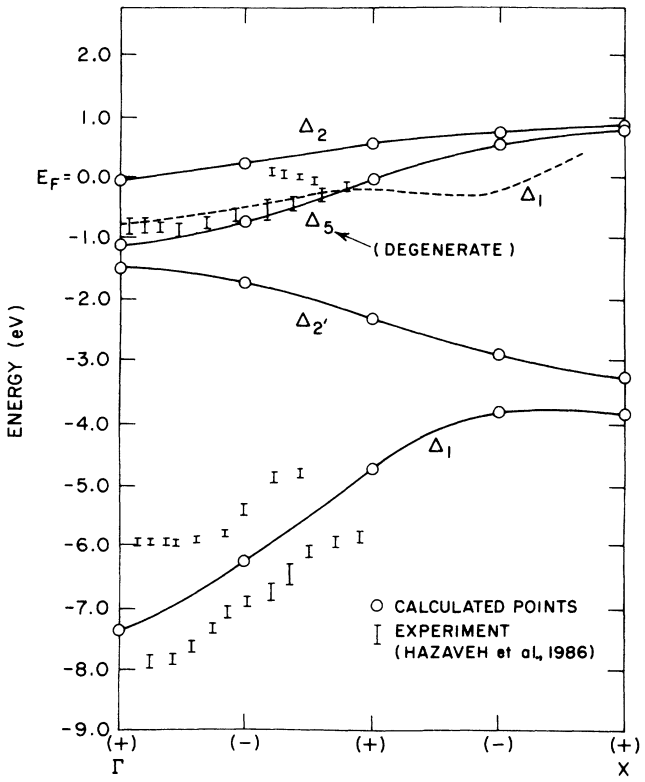

FIG. 6. A comparison of the film-derived bulk bands along Δ with the experimental results reported in Ref. 8. The open circles denote the states at $\bar{\Gamma}$ calculated for our paramagnetic, five-layer fcc iron film. The solid lines are a guide to the eye. The dashed line connects calculated states (not shown here) that have been strongly affected by the surface compared to a bulk calculation. The vertical bars refer to experimental data from Ref. 8. The symmetry labels identifying the bands are also shown.

stant. It is also interesting to note the above small change in total charge in spite of fairly large magnetic moments seen in the spin-polarized calculation. The conclusions that can be drawn here are the following. (1) A large exchange splitting and an associated large moment at the surface do not necessarily induce a large change in work function. (2) Electrons inside the surface muffin-tin sphere have only a small effect on the work function. What must be most important in determining the work-function changes is the electron density around and beyond the surface muffin-tin radius.

We also note that our calculated work functions agree quite well with those calculated by Fu and Freeman.[20] For two layers of ferromagnetic iron on Cu(001), they report a work function of 4.95 eV, while our calculations yield a work function of 5.1 eV for a five-layer film of fcc Fe(001) with ferromagnetic coupling between the surface and the subsurface layers that are antiferromagnetically coupled to the center layer.

D. Magnetic moments and total energies

The behavior of the magnetic moments during the self-consistent procedure is worth noting. We started the self-consistent calculation for the five-layer fcc iron magnetic film, as is usually done, using a fully-self-consistent paramagnetic potential. The first few starting iterations were done with an artificial splitting (as described in Sec. II) favoring ferromagnetic coupling between all layers. Then the artificial splitting was removed and the system was allowed to evolve by itself. The magnitudes of the magnetic moments started to increase and kept on increasing until the center, subsurface, and surface moments were about $0.5\mu_B$, $0.6\mu_B$, and $1.3\mu_B$, respectively, with ferromagnetic coupling between all layers. The system appeared to be close to self-consistency. We were using Broyden[19] or straight mixing of $\rho^{\uparrow}$ with $\rho^{\uparrow}$ from earlier iterations and $\rho^{\downarrow}$ with $\rho^{\downarrow}$ from earlier iterations, and small mixing parameters. At this point we employed a different mixing scheme where the quantities mixed were (charge densities) $\rho^{\uparrow}+\rho^{\downarrow}$ with $\rho^{\uparrow}+\rho^{\downarrow}$ from earlier iterations and (spin densities) $\rho^{\uparrow}-\rho^{\downarrow}$ with $\rho^{\uparrow}-\rho^{\downarrow}$ from earlier iterations. This enabled us to use a large (about 50% or more) mixing parameter β [as in Eq. (2.4)] for the spin density and a smaller mixing of the charge density with straight or Broyden mixing. With the introduction of

TABLE I. Layer-projected valence charges and magnetic moments together with the work functions of paramagnetic and magnetically ordered fcc iron five-layer slabs and paramagnetic monolayer of iron on a five-layer Cu(001) slab. The values in parentheses are for the (2%) relaxed Fe/Cu(001) system. Note that for the five-layer iron slabs in the first two columns the next-to-center and subsurface layers are the same.

		fcc iron (paramagnetic)	fcc iron (magnetically ordered)	Fe/Cu(001) (paramagnetic)
Valence (electrons):	Center	7.20	7.20	(10.32) 10.32
	Next to center	7.16	7.17	(10.33) 10.33
	Subsurface			(10.36) 10.34
	Surface	6.98	6.96	(6.87) 6.95
Net moment (μ_B):	Center		1.68 (↓)	
	Subsurface		2.30 (↑)	
	Surface		2.79 (↑)	
Work function (eV):	Present theory	5.3	5.1	(5.5) 5.6
	Experiment (Refs. 6 and 7)	5.4	5.0	5.5

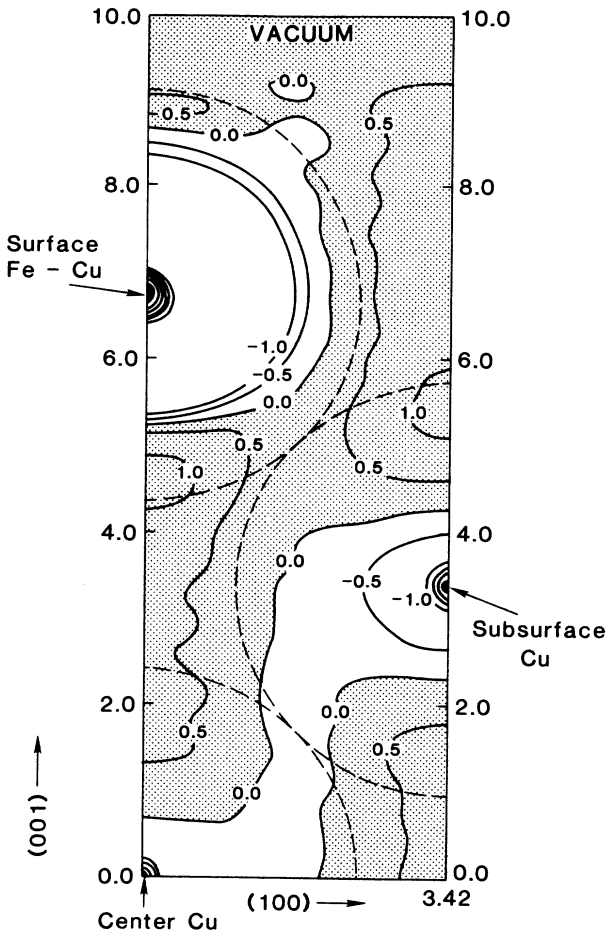

FIG. 7. A difference-electron-density contour plot of fcc Fe(001) and fcc Cu(001). This plot has been obtained by subtracting our (self-consistently) calculated fcc Cu(001) five-layer film electron density from our calculated Fe/Cu(001)-film electron density by aligning the surface layers. It should be used to compare differences in electronic density between the Cu(001) surface and the Fe/Cu(001) surface. The contours are labeled in units of 0.01 electrons/a_0^3. The numbers along the vertical and horizontal axes refer to distances in Bohr radii. The shaded regions show areas with increased electronic density. This change helps explain the work-function increase calculated in going from five layers of Cu(001) to five layers of Fe(001), both paramagnetic.

this mixing scheme the center-layer moment started decreasing in magnitude, went through zero, and ended up at the value shown in Table I with a moment opposite to the ones in the surface and subsurface layers. The way we interpret this is as follows. When the mixing parameter was small, the system was almost trapped in a metastable local minimum with ferromagnetic coupling between all layers. However, with a large mixing of the spins the system was able to move out of this local minimum and proceed towards the global (absolute) minimum, which has the antiferromagnetic coupling between center and subsurface, but ferromagnetic coupling between subsurface and surface, as shown in Table I.

Total-energy calculations allow us to directly test the theoretical understanding of the ground-state properties of a system. Our calculated total energy of the magnetic state described above is lower than that of the paramagnetic state by about 0.100 Ry. This shows that within the local-spin-density approximation the ground state of fcc iron grown on Cu(001) should be magnetic with the magnetic ordering given in Table I. Our results are consistent with those in Ref. 20, where for five layers of fcc iron covered by two layers of copper on either side, the $++-$ structure (the same sequence of ferromagnetic and antiferromagnetic coupling as we get for five layers of fcc Fe) is the ground state, 0.78 eV below the paramagnetic state. Our results clearly predict surface ferromagnetism (with a moment of $2.79\mu_B$) for iron grown on Cu(001). Our results also suggest the possibility of having an antiferromagnetic interior (moment $1.68\mu_B$). The antiferromagnetic nature of the interior could be further verified by a thicker (seven-layer) fcc-iron-slab calculation. Inclusion of any surface expansions in our fcc iron calculation as seen in the LEED experiments[6,7] will tend to favor the magnetically ordered state even more.

E. Contact hyperfine fields

The contact hyperfine field, which is due to the electron polarization at a particular nucleus, can be measured through Mössbauer spectroscopy. In Table II we show our calculated contact fields in kG separated into core and valence (4*s*) contributions. Here we note that the contact field at the center-layer nucleus is very much smaller than those at the surface and subsurface. The core and 4*s* valence densities at the center-layer nucleus are polarized roughly equally, but in opposite directions, almost canceling each other. There is some experimental support to the trend seen in Table II. The Mössbauer work of Ref. 10 has seen a reduction of the contact fields in the inner layers of iron on Cu(001) compared to the surface. This study concludes that the low-temperature (4K) magnetic state of these films is antiferromagnetic, which is also consistent with our total-energy calculations. Finally, as has now been established,[21] the ratio between the contact field due to core electrons and the magnetic moment of that particular atom stays almost constant here.

TABLE II. Fermi contact hyperfine fields in kG, separated into core and valence contributions for various layers of the fcc iron slab. Note that the total contact field at the center-layer nucleus is significantly lower than those at the surface and subsurface. The last row gives the ratio between the core contribution to the contact field and the magnetic moment.

	Center	Subsurface	Surface
Core	+209	−294	−359
Valence (4*s*)	−223	+39	+80
Total	−14	−255	−279
Core field/moment (kG/μ_B)	124	128	129

IV. COMPARISON WITH EXPERIMENT AND DISCUSSION

A. Experimental situation

The nature of the magnetic state of fcc iron on Cu(001) at room temperature has been a controversial issue. Recent ultraviolet-photoemission-spectroscopy (UPS) data together with surface magnetooptic Kerr effect (SMOKE) results led to the view that the room-temperature state of Fe/Cu(001) is paramagnetic.[6,7] There is also an angle-resolved ultraviolet-photoemission (ARUPS) study[8] which supports this conclusion. However, papers reporting a spin-resolved photoemission study[5] and an ARUPS study, together with a calculated band structure,[3] claim that the room-temperature state of fcc Fe(001) on Cu is ferromagnetic. There are reported Mössbauer-spectroscopy experiments which show the absence of magnetism at room temperature and the presence of antiferromagnetism at very low (4 K) temperatures.[10] There is clearly no general agreement as to the nature of the room-temperature magnetic state and we will try to address this issue as we discuss some of the above experimental data with respect to our calculated results in this section.

Surface magnetooptic Kerr effect results of Refs. 6 and 7 showed the absence of ferromagnetism parallel to the surface at room temperature. These were supported by photoemission results[6,7] which failed to detect any clear splitting of the spectra at room temperature. While these photoemission results by themselves do not provide any conclusive evidence as to the nature of the magnetic state at room temperature, the SMOKE results do. Thus we have a situation where our calculated total-energy results, which show a magnetic ground state, may be in disagreement with the SMOKE measurements.

However, the absence of ferromagnetism at room temperature as found in Refs. 6 and 7 and, hence, the possible disagreement with our calculations may be explained as due to one of the following: (a) Perhaps the local-spin-density-functional theory cannot describe these magnetic exchange and correlation effects accurately enough (or there is a similar defect in the theory), or (b) these fcc iron films have an ordering temperature below room temperature, or (c) the magnetism in these samples has been quenched by some impurities, or (d) the magnetic moment lies perpendicular to the surface of the film and hence is undetectable in the SMOKE geometry used in the experiment. The measurements on these samples were done in ultrahigh vacuum and hence were free of any detectable impurities at the presently attainable levels of technology. There is some experimental evidence[5] that the moments can lie perpendicular to the surface at 30 K, but at room temperature it is unlikely that the iron film can sustain a large enough asymmetric field to keep the moments perpendicular to the surface. That leaves us with (a) and (b) as possible explanations of the room-temperature results of Refs. 6 and 7.

B. Ultraviolet photoelectron spectroscopy (UPS) and calculated density of states

Any direct comparison of calculated band structure or DOS (density of states) with photoemission experiments is known to contain certain systematic errors. The local-density (or spin-density) approximation used in band calculations such as ours allows the electron to interact with itself, thereby pushing the calculated eigenvalues to higher binding energies. In photoemission, although the measurement desired is of ground-state properties, the hole created is screened by the nearby electrons and, hence, there are relaxation effects associated with the measured binding energies. These relaxation effects and the self-interaction effects act in opposite directions and, hence, sometimes cancel each other. It is also questionable whether different l (s, p, d, etc.) components of the charge density can correctly be described by the same local correlation functional based on the homogeneous electron gas.[22] Many-body effects in transition metals have been recognized as important in understanding photoemission results. For example, in an angle-resolved photoemission experiment[23] on Ni, the observed exchange splitting is only half the value calculated using local-spin-density-functional theory. However, a similar comparison for iron showed fair agreement.[24] It should be understood that whenever there is reasonable agreement between a calculated band structure and experimental bands, the many-body effects as well as thermal effects are either insignificant or have canceled each other. Although it is generally believed that the local-density theory gives the best state of the art zero-temperature results compared to any other phenomenological theory, the subject is far from being closed.

We have carried out some detailed comparisons of our calculated bands and DOS with experiment. The angle-integrated UPS (ultraviolet photoemission) study in Refs. 6 and 7 using He I radiation (at 21.2 eV) finds a bulklike fcc iron feature in the photoemission spectra about 1.1 eV below the Fermi level. Our calculated paramagnetic DOS (Fig. 1) shows a feature slightly below the above value in energy. This feature is present in all layers and is sharpest in the center-layer DOS, which is consistent with the experimental observation. In order to understand the magnetic nature of the fcc iron films grown on Cu(001), we have compared the experimental EDC's (energy-distribution curves) with our spin-polarized DOS curves (Fig. 3). The feature mentioned above is still seen, though at a slightly more negative energy, and again it is sharpest in the center-layer DOS, but present in all layers. For this reason, it is not possible to make a clear identification whether the fcc iron films grown on Cu(001) are magnetic or nonmagnetic using the comparison of angle-integrated photoemission spectra[6,7] with the calculated DOS.

C. Comparison with angle-resolved ultraviolet-photoemission-spectroscopy (ARUPS) data

To our knowledge there are two ARUPS (angle-resolved ultraviolet photoemission) experiments reported in the literature for Fe grown on Cu(001). In one study[3] a comparison is made with a spin-polarized band calculation based on the linearized augmented-plane-wave (LAPW) method. This study treated the two-dimensional (2D) surface band structure, i.e., for one and two layers of

Fe on Cu(001). The other study[8] maps out some bulk bands along Δ for fcc Fe on Cu(001). Neither of these experiments are spin resolved and hence are of limited value in reaching conclusions regarding the magnetic state of the epitaxially grown iron. Since our calculations yield the 2D band structure of fcc iron films grown on Cu(001), we will first discuss the surface study.[3] In this experiment ARUPS bands along $\bar{\Delta}$ and $\bar{\Sigma}$ in the vicinity of the Fermi level have been mapped out for one and two monolayers of iron on Cu(001) at room temperature. A comparison with a film spin-polarized calculation is reported[3,20] to have good agreement with the experimental bands, although certain disagreements exist. The general conclusion of Ref. 3 and later in Ref. 20 seems to be that the fcc iron grown on Cu(001) at room temperature is ferromagnetic.

In Fig. 8 we show a comparison of our calculated spin-polarized bands for a five-layer slab of fcc Fe(001)

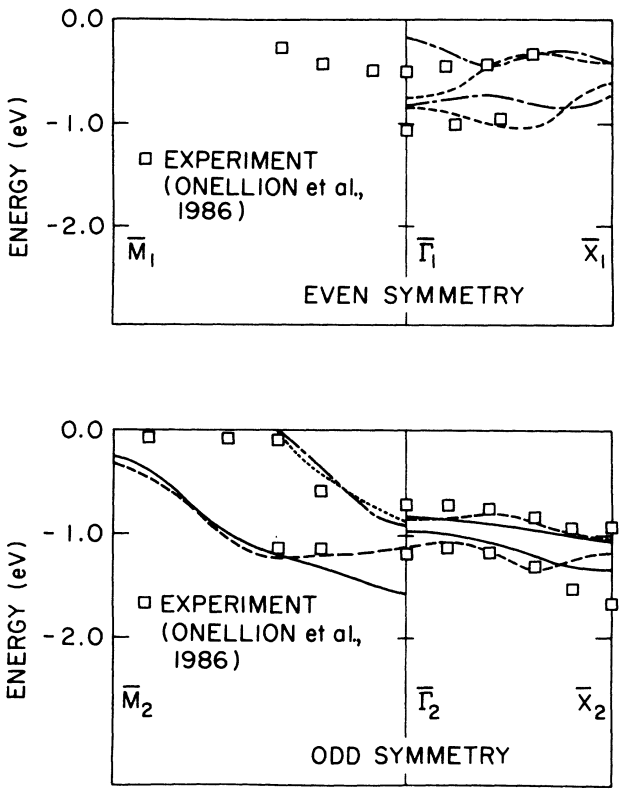

FIG. 8. A comparison of our calculated spin-polarized bands with ARUPS data of Ref. 3. The open squares are the experimental data of Ref. 3. The upper panel (even-symmetry in plane containing symmetry direction being spanned) shows two pairs of calculated minority bands in $+z$ reflection symmetry (short-dashed lines) and $-z$ reflection symmetry (long-dashed–short-dashed lines). The lower panel (odd-symmetry in plane) shows four pairs of our calculated bands, with solid and long dashed lines showing majority bands in $+$ and $-$ z reflection symmetries, respectively, while the short-dashed and long-dashed–short-dashed lines show minority bands in $+$ and $-$ z reflection symmetries, respectively. All the calculated bands shown here contain at least one state with 40% or more surface Fe weight.

with the experimental data of Ref. 3. The bands shown in Fig. 8 are identical to those in the same energy region in Figs. 5(b) and 5(c) as discussed below, where both the heavily and lightly drawn band sections of Figs. 5(b) and 5(c) are included in Fig. 8. Note the presence of *pairs* of calculated surface-dominant bands, which is due to having two surface atoms (one on each side of the slab) in our calculations. This point will be discussed further in subsection E below. The agreement in this case is reasonable with one serious exception, which is the absence of a heavily-surface-dominant calculated pair of bands having the experimental dispersion along $\bar{\Sigma}$ in even symmetry. When our paramagnetic bands shown in Fig. 4 are compared with the same experimental data, we again see somewhat reasonable agreement, but not for all the compared bands. In our calculated spin-polarized odd-symmetry bands [Figs. 5(c) and 5(d)], we have identified two pairs of majority surface bands [Fig. 5(c)] ($+$ and $-z$ reflection) along $\bar{\Delta}$ in the region of comparison (close to 1 eV below E_F). Heavily surface-dominated bands are absent in the minority spins here [Fig. 5(d)]. In the paramagnetic case in odd symmetry along $\bar{\Delta}$ [Fig. 4(b)], one pair of bands is seen around 1 eV below the Fermi level, while the other pair is close to the Fermi level at $\bar{\Gamma}$. However, their surface content is not as strong as that seen in the spin-polarized case. In even symmetry along $\bar{\Delta}$ we have identified two pairs of minority-spin bands [Fig. 5(b)] in the region of comparison (between about 1 eV below E_F and E_F). However, our paramagnetic results [Fig. 4(a)] also show two pairs of bands here. A similar comparison made along the $\bar{\Sigma}$-symmetry direction also shows that there are bands in paramagnetic as well as magnetic cases which compare favorably with the ARUPS-derived bands. Our paramagnetic Fe/Cu(001) bands (not shown here) also show somewhat similar placement. Hence at the level of uncertainty and disagreements present in this comparison, one cannot conclusively make a decision on the magnetic nature of iron grown on Cu(001).

The other ARUPS study[8] measures bands along Δ for bulk fcc iron grown on Cu(001). We have already discussed some of the features of our paramagnetic "*film-derived bulk bands*" shown in Fig. 6. The experimental data of Ref. 8 are shown as vertical bars in this figure. An important observation in the work of Hazaveh *et al.*[8] is the absence of a (magnetically) split Δ_5 band. The band with Δ_5 symmetry, which shows a large exchange splitting[25] in bcc iron, does not show any splitting to within the experimental resolution of 0.3 eV for fcc Fe grown on Cu(001) at room temperature. There is general agreement between theory and experiment, except for the fact that we are unable to produce a feature (the second experimental band from the bottom in Fig. 6) seen around -6 eV in this study, which the authors of Ref. 8 suggest may be due to many-body effects. The authors rule out possible oxygen contamination using Auger spectroscopy; however, it is important to understand definitively the origin of this -6-eV feature, as any surface contamination could easily lead to a reduction in the exchange splitting.

There is a spin-polarized photoemission study[5] on this

system which identifies a ferromagnetic moment perpendicular to the iron surface at 30 K. This study identifies ferromagnetism at the surface for one, three, and five layers of iron on Cu(001) with the direction of alignment changing from perpendicular to parallel above 30 K. The ordering temperatures reported are 230 K for the monolayer film and 390 K for the thicker films, with an uncertainty of about 30 K. This study clearly suggests that the Curie temperature of thick iron films on Cu(001) is somewhat higher than room temperature. The ordering temperature could be sensitive to film preparation and hence the above work and Refs. 6 and 7 are not necessarily in complete disagreement as to the nature of the room-temperature state. More spin-resolved studies would be very welcome here. Spin-polarized angle-resolved data to see whether there is any splitting of the Δ_5 band and electron-capture experiments as done[4] for Fe/Cu(111) should provide important clues. These should be done over a range of temperatures since there are indications of thermally driven, magnetic transitions.

D. Magnetic state at 460 K

The experiment in Refs. 6 and 7 yields a ferromagnetic state at 460 K with moment parallel to the film plane, compared to the absence of such ferromagnetism parallel to the plane at room temperature. The well-defined surface magnetooptic Kerr effect (SMOKE) hysteresis pattern and the splitting seen in photoemission were transient phenomena disappearing in about 1 h. Cooling to 323 K also resulted in a loss of SMOKE hysteresis, and the original signals did not reappear when the samples were reheated. Fresh deposits of iron at 460 K showed a clear SMOKE signal indicating ferromagnetism, with an intensity, however, corresponding only to the surface layer. We believe that a theoretical explanation of this magnetic state goes beyond the scope of our zero-temperature electronic-structure calculations. The time-dependent nature of this magnetic state and the lack of reversibility suggest that this is a thermally driven, first-order magnetic transition to a state that is metastable with respect to the state that is stable at room temperature. Face-centered-cubic iron has been predicted to undergo various magnetic transitions depending on the lattice parameter (see Refs. 11–16). However, none of the band calculations has any temperature effects included, and their relevance in this situation is not clear. While frankly seeing no justification for relevance, we will still point out some interesting resemblances between our magnetically ordered ground state and the high-temperature magnetic state seen for these iron films. The SMOKE results[6,7] indicate that the ferromagnetism at 460 K is limited to the surface. Our calculated magnetic state has a ferromagnetic surface but an antiferromagnetic interior, and there would be no SMOKE intensity for antiferromagnetism. Hence our calculated results for the ground state are compatible with the experimental state at 460 K. The work-function measurements[7] for the magnetic state also are consistent with our calculations for the magnetically ordered state, although, as mentioned earlier, caution should be exercised in attaching significance to this. On the other hand, the apparent exchange splitting seen for the magnetic state in the angle-integrated UPS experiment[7] is certainly very much lower than the calculated average exchange splitting, which is about 2 eV in the energy range of interest.

E. Comparison with other calculations

There are some peculiarities in the thin-film calculations on Fe/Cu(001) reported in Refs. 3 and 20, although our calculations agree with their predictions of the ground state, and the work function. The slab geometry for these calculations, as well as for ours, is such that there are two surface atoms in the unit cell, one on each side of the slab. This leads to a pair of calculated bands (here in $+$ and $-z$ reflection symmetry) for any experimentally determined surface band. However, some relevant bands in Refs. 3 and 20 do not show this behavior. For example, in at least one direction (i.e., along $\bar{\Delta}$) the calculated results (see Figs. 3 and 4 of Ref. 20) do not have the correct number (four) of odd bands to compare with the two experimentally measured bands in the energy range of comparison (0–1.8 eV below the Fermi level).

In a thin-film calculation these $+$ and $-$ z-reflection-symmetry bands split, depending on (a) whether the two opposite surface orbitals directly interact, or (b) whether these orbitals hybridize with others from the interior that are subject to z-reflection-symmetry restrictions. The surface bands in the limit of infinite film thickness (and hence more closely related to the experimental situation) should be extrapolated as lying around the center of gravity of the calculated $+$ and $-$ z reflection bands corresponding to finite films as this is probably the best estimate one can give. When there are *"missing bands"* in the energy range of comparison as in Refs. 3 and 20, the placement of the bands that are shown become questionable. It could also be argued that the level of agreement with the experimental band structure is also present in paramagnetic calculations, as we have discussed earlier. In view of the above discussion, the validity of the comparison shown in Ref. 3 of the calculated and experimental bands is not clear to us.

V. CONCLUDING REMARKS

At present there are two sets of detailed calculations of the electronic and magnetic structure of fcc iron as grown on Cu(001), our own as reported here and briefly earlier[7] that of Fu and Freeman.[20] The overall nature of the ground state predicted by these two sets of calculations seems to be in basic agreement. Both predict surface ferromagnetism coupled to bulk antiferromagnetism. The surface and bulk moments predicted, and the energy advantage (relative to a paramagnetic state) of the magnetically ordered ground state, are in reasonably good agreement for the two sets of calculations. On the other hand, we question the absence of certain pairs of bands artificially introduced by the use of slab geometry in the one-electron (spectroscopic) behavior predicted in Ref. 20 (or by the same authors in the theoretical part of Ref. 3).

With regard to comparison with experiment, we are confronted with a thicket of oddities and contradictions in the experimental data. Above, we have discussed comparisons of our calculated results to various aspects of the

experimental behavior as found by different investigators. It appears likely that sensitivity to lattice spacing plays a crucial role in the magnetic state of fcc Fe on Cu(001). Deciding whether or not the experimental behavior can be understood on the basis of local-spin-density–approximation calculations, such as our own, will first require confidence that several experimental investigators are obtaining the same spectroscopic and magnetic behavior with consistent temperature dependencies. A particularly valuable type of new data would be to have *spin-polarized* angle-resolved photoemission data.

ACKNOWLEDGMENTS

We have benefited throughout the development of this work by discussion of the experimental research with P. A. Montano and S. D. Bader. We would like to thank J. W. Davenport for pointing out a spin-mixing scheme to improve the rate of convergence. The research at Brookhaven National Laboratory has been supported by the Division of Materials Sciences, Office of Basic Energy Sciences, U. S. Department of Energy, under Contract No. DE-AC02-76CH00016. The research at Los Alamos National Laboratory and West Virginia University has been supported by the U. S. Department of Energy and by the West Virginia University Energy Research Center. We are indebted to the Pittsburgh Superconducting Center–National Science Foundation and to the Center for Materials Science at Los Alamos National Laboratory for supplying the time on Cray supercomputers necessary for the computations described in this paper.

[1]H. Hasegawa and D. G. Pettifor, Phys. Rev. Lett. **50**, 130 (1983).
[2]G. J. Johanson, M. B. McGirr, and D. A. Wheeler, Phys. Rev. B **1**, 3208 (1970).
[3]M. F. Onellion, C. L. Fu, M. A. Thompson, J. L. Erskine, and A. J. Freeman, Phys. Rev. B **33**, 7322 (1986).
[4]C. Rau, C. Schneider, G. Xing, and K. Jamison, Phys. Rev. Lett. **57**, 3221 (1986).
[5]D. Pescia, G. L. Bona, A. Vaterlaus, R. F. Willis, and F. Meier, Phys. Rev. Lett. **58**, 2126 (1987).
[6]G. W. Fernando, Y. C. Lee, P. A. Montano, B. R. Cooper, E. R. Moog, H. M. Naik, and S. D. Bader, J. Vac. Sci. Technol. A **5**, 882 (1987).
[7]P. A. Montano, G. W. Fernando, B. R. Cooper, E. R. Moog, H. M. Naik. S. D. Bader, Y. C. Lee, Y. N. Darici, H. Min, and J. Marcano, Phys. Rev. Lett. **59**, 1041 (1987).
[8]A. Amiri Hazaveh, G. Jennings, D. Pescia, R. F. Willis, K. Prince, M. Surman, and A. Bradshaw, Solid State Commun. **57**, 329 (1986).
[9]W. Becker, H. D. Pfannes, and W. Keune, J. Magn. Mater. **35**, 53 (1983).
[10]R. Halbauer and U. Gonser, J. Magn. Mater. **35**, 55 (1983).
[11]J. Kübler, Phys. Lett. **81A**, 81 (1981).
[12]O. K. Andersen, J. Madsen, U. K. Poulsen, O. Jepsen, and J. Kollar, Physica **86-88B**, 249 (1977).
[13]D. Bagayoko and J. Callaway, Phys. Rev. B **28**, 5419 (1983).
[14]V. L. Morruzi, Phys. Rev. Lett. **57**, 2211 (1986).
[15]F. J. Pinski, J. Staunton, B. L. Gyorffy, D. D. Johnson, and G. M. Stocks, Phys. Rev. Lett. **56**, 2096 (1986).
[16]C. S. Wang, B. M. Klein, and H. Krakauer, Phys. Rev. Lett. **54**, 1852 (1985).
[17]G. W. Fernando, B. R. Cooper, M. V. Ramana, H. Krakauer, and C. Q. Ma, Phys. Rev. Lett. **56**, 2299 (1986); C. Q. Ma, M. V. Ramana, B. R. Cooper, and H. Krakauer, Phys. Rev. B **34**, 3854 (1986).
[18]S. H. Vosko, L. Wilk, and N. Nusair, Can. J. Phys. **58**, 1200 (1980).
[19]G. P. Srivastava, J. Phys. A **17**, L317 (1984).
[20]C. L. Fu and A. J. Freeman, Phys. Rev. B **35**, 925 (1987).
[21]A. J. Freeman and R. E. Watson in *Magnetism,* edited by G. T. Rado and H. Suhl (Academic, New York, 1965), Vol. II A.
[22]O. Gunnarsson and R. O. Jones, Phys. Rev. B **31**, 7588 (1985).
[23]F. J. Himpsel, J. A. Knapp, and D. E. Eastman, Phys. Rev. B **19**, 2919 (1979).
[24]D. E. Eastman, F. J. Himpsel, and J. A. Knapp, Phys. Rev. Lett. **44**, 95 (1980).
[25]E. Kisker, K. Schröder, W. Gudat, and M. Campagna, Phys. Rev. B **31**, 329 (1985).

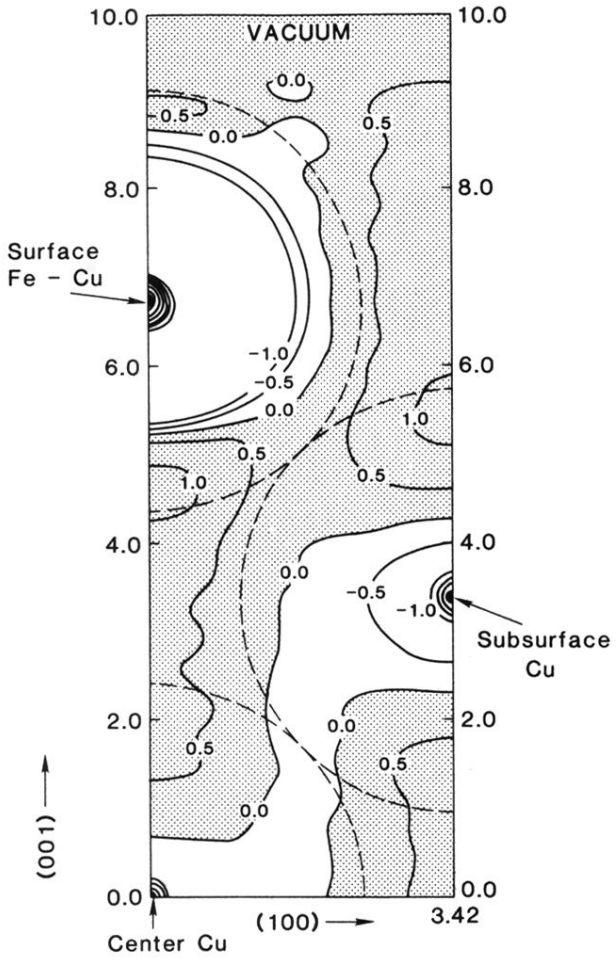

FIG. 7. A difference-electron-density contour plot of fcc Fe(001) and fcc Cu(001). This plot has been obtained by subtracting our (self-consistently) calculated fcc Cu(001) five-layer film electron density from our calculated Fe/Cu(001)-film electron density by aligning the surface layers. It should be used to compare differences in electronic density between the Cu(001) surface and the Fe/Cu(001) surface. The contours are labeled in units of 0.01 electrons/a_0^3. The numbers along the vertical and horizontal axes refer to distances in Bohr radii. The shaded regions show areas with increased electronic density. This change helps explain the work-function increase calculated in going from five layers of Cu(001) to five layers of Fe(001), both paramagnetic.